Impact of Chlorophyll Shading on the Peruvian Upwelling System

Vincent Echevin, Jaard Hauschildt, François Colas, Soeren Thomsen, Olivier Aumont

Geophysical Research Letters®

Impact of Chlorophyll Shading on the Peruvian Upwelling System

V. Echevin[1] [ID], **J. Hauschildt[2]**, **F. Colas[1]** [ID], **S. Thomsen[1]** [ID], **and O. Aumont[1]** [ID]

[1]Sorbonne Université, LOCEAN-IPSL, CNRS/IRD/MNHN, Paris, France, [2]GEOMAR Helmholtz Centre for Ocean Research Kiel, Kiel, Germany

Abstract The influence of chlorophyll shading on ocean dynamics has been usually disregarded in eastern boundary upwelling systems modeling studies in spite of their very high primary productivity. Here, we study how this effect impacts on the Peru upwelling system using a regional mesoscale-resolving physical biogeochemical coupled model. We show that the shading effect leads to a surface cooling of up to 1°C on the shelf due to subsurface cooling of the source waters during their transit toward the shelf. The shading effect leads to a more realistic subsurface stratification, a slowdown of the alongshore currents, and a shoaling of the oxycline. Impacts on the regional model biases show that the shading effect needs to be taken into account in both physical and coupled physical-biogeochemical regional models of upwelling systems.

Plain Language Summary The chlorophyll pigments of phytoplankton capture the downward penetrating solar energy to produce photosynthesis and warm the surface of the ocean. However, this effect is seldom taken into account in ocean models, in particular in upwelling systems where chlorophyll concentration is very high. In this study, we show that taking into account this effect in a model of the Peruvian upwelling system, one of the most productive systems in the world, modifies not only the temperature, circulation, and turbulence, but also stimulates nearshore phytoplankton production and deoxygenation over the shelf. This study shows that this effect needs to be parameterized in future modeling studies.

1. Introduction

Eastern Boundary Upwelling Systems (EBUS) are among the most productive oceanic systems (Messié & Chavez, 2015). There, the coastal upwelling of cold, nutrient-rich subsurface waters triggers intense phytoplankton blooms. Since about two decades, progress in regional ocean modeling has led to an increasingly realistic representation of EBUS dynamical and biogeochemical processes (e.g., Gruber at al., 2006; Kessouri et al., 2020; Marchesiello et al., 2003 for the Californian EBUS; Colas et al., 2012; Espinoza-Morriberon et al., 2019; Hauschildt et al., 2021; Montes et al., 2010, 2014; Penven et al., 2005 for the Peruvian EBUS). Improvements were partly due to the Regional Ocean Modeling System (ROMS, Shchepetkin & McWilliams, 2005) being able to simulate the mesoscale and submesoscale dynamics. However, in spite of the EBUS high phytoplanktonic biomass, the biophysical effects of the absorption of solar radiation by chlorophyll pigments (hereafter called the "shading effect") on the dynamics has not been studied in a realistic eddy-resolving modeling framework. In previous regional modeling studies, heating by absorption of shortwave solar radiation relies on the assumption that oligotrophic, low chlorophyll waters (Chl < 0.01 mg Chl m^{-3}) are present everywhere in the model domain. Consequently, subsurface solar heating occurred at unrealistic too large depths.

Previous studies documented the shading effect in upwelling regions using relatively coarse resolution models. Hernandez et al. (2017) found a cooling of the sea surface temperature and a shoaling of the mixed layer depth in the Benguela and Canary upwelling systems using a 0.25° ocean model in which the shading effect was produced by prescribed chlorophyll profiles. Simulating the equatorial Pacific with an eddy-permitting (0.25°) regional ocean model coupled to a simple biogeochemical model, Loeptien et al. (2009) found a cooling of ~1°C (leading to a reduction of the model surface temperature bias) in the Peru upwelling region associated to the shading effect. On the other hand, contrasted dynamical responses to the shading effect have been found in the equatorial Pacific using a variety of low-resolution (1–2°) global ocean-only and

ocean-atmosphere coupled models to investigate the effect of ENSO dynamics (e.g., Park et al., 2014 for a review). While most models simulated a cooling of ~0.5°C–1°C in the Peru upwelling region (e.g., Anderson et al., 2007; Lin et al., 2007; Manizza et al., 2005), a warming of the eastern Pacific (~0.4°C) was produced in a fully coupled ocean-atmosphere-biogeochemical simulation (Lengaigne et al., 2007). Note that the Peru coastal upwelling dynamics is not well resolved in these models due to their coarse horizontal resolution.

In the present study, we investigate the impact of the shading effect on the Peru EBUS dynamics. This system hosts the most productive small pelagic fisheries (FAO, 2017) and an intense and particularly shallow Oxygen Minimum Zone (OMZ; e.g., Paulmier & Ruiz-Pino, 2009). We evaluate the impact on sea surface temperature (SST), stratification, nearshore currents, and key biogeochemical variables (surface chlorophyll content, nutrient, and dissolved oxygen) using a high-resolution (1/12°, ~10 km) eddy-resolving coupled biophysical regional model.

2. Materials and Methods

2.1. Hydrodynamical Model

We use the CROCO (Coastal and Regional Ocean Community, Hilt et al., 2020) model to simulate ocean dynamics. CROCO is the ocean modeling platform built upon ROMS_AGRIF (Penven et al., 2006). It solves the primitive equations based on the Boussinesq and hydrostatic approximations. The vertical dimension is discretized in terrain-following coordinates. Horizontal advection of temperature and salinity is performed using a third-order scheme and diffusion is represented by a rotated biharmonic diffusion scheme along isopycnal surfaces (RSUP3; Lemarié et al., 2012). Horizontal advection of biogeochemical tracers is performed using the quasi-monotone WENO5 scheme to avoid the generation of negative values. Vertical mixing is parameterized using KPP (Large et al., 1994). The optical model used to represent the propagation and absorption of solar energy in the water column is a two-waveband model (Paulson & Simpson, 1977; see Supporting Information S1) in which the water is by default assigned to the most transparent Jerlov type I (Chl < 0.01 mg m^{-3}).

The model domain extends from 22°S to 5°N in latitude and from 96°W to 70°W in longitude, with 10 km horizontal resolution and 64 sigma levels. Bottom topography from STRM30 (Becker et al., 2009) is interpolated on the grid and smoothed in order to reduce potential errors in the horizontal pressure gradient. The reader is referred to Shchepetkin and McWilliams (2003) and to Shchepetkin and McWilliams (2005) for a more complete description of the model parameterizations.
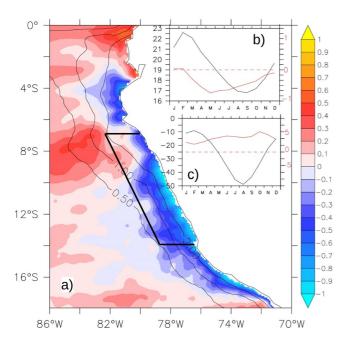
2.2. Biogeochemical Model

The PISCES biogeochemical model (Pelagic Interaction Scheme for Carbon and Ecosystem Studies; Aumont & Bopp, 2006; Aumont et al., 2015) is coupled to CROCO. PISCES simulates the marine biological productivity and biogeochemical cycles of carbon, nutrients (nitrate, phosphate, silicate, and iron), and dissolved oxygen (DO). It includes a three-waveband (red: 600–700 nm; green: 500–600 nm; blue: 400–500 nm) spectral model to compute light availability depending on depth and chlorophyll concentration (see Hernandez et al., 2017; Lengaigne et al., 2007, for details; Figure S1). In this study, the spectral model is used to compute light limitation for the phytoplankton growth rate as well as heating of the water mass in the "chlorophyll shading" simulation (hereafter SH). In contrast, heating is computed assuming Jerlov I water type (i.e., clear water; Jerlov, 1976) with similar depth-dependent absorption coefficients everywhere in the "no-shading" standard simulation (hereafter NSH).

2.3. Model Atmospheric and Open Boundary Forcing

Both simulations are forced by a monthly climatological wind stress computed from the Advanced Scatterometer (ASCAT, 1/4° resolution) over 2008–2015 and by COADS climatological net, shortwave heat fluxes, and freshwater fluxes (DaSilva et al., 1994). Model sea surface temperature (SST) is relaxed to observed climatological SST (2008–2015) derived from the merged multisensor OSTIA product (Donlon et al., 2012) following Barnier et al. (1995). Typically, a corrective heat input of ~40 W m^{-2} is forced into the surface mixed layer with a time scale of ~35 days when model SST becomes 1°C cooler than climatological SST.

Figure 1. (a) Annual mean sea surface temperature (SST) difference (SH-NSH; in °C; color scale) and surface chlorophyll (NSH; in mg Chl m^{-3}; contour lines). (b) Evolution of the SST (NSH, black line) and of the SST difference (SH-NSH, red line) in the coastal box (delimited by black lines); (c) same as (b) for the mixed layer depth.

Open boundary conditions (OBC) of the regional model are derived from a climatology of GLORYS2V4 reanalysis (1/4°; Ferry et al., 2012) over the period 2008–2015 for T, S, U, V, and SSH. Biogeochemical OBC are imposed using the CARS2009 climatology (Ridgway et al., 2002) for macronutrients and DO, the Global Ocean Data Analysis Project (GLODAP; Key et al., 2004) data base for dissolved inorganic carbon and total alkalinity, and a global PISCES simulation (Aumont & Bopp, 2006) for iron and dissolved organic carbon. Climatological atmospheric dust deposition (Tegen & Fung, 1995) and a depth-dependent sediment flux provide iron to the water column (Aumont et al., 2015).

First, a climatological simulation without shading initialized with GLORYS2v4 is run for 6 years as a spin-up. Then NSH and SH simulations are initialized using the same initial state (final state of the spin-up phase) and run for 10 years. The last seven years are used to build the analyzed climatology.

2.4. Lagrangian Tracking of the Upwelled Water Masses

The impact of the shading effect on the circulation may modify the pathways of the water masses that are upwelled near the coast. In order to track these changes, virtual Lagrangian floats are released in a 100-km-wide, 20-m-thick surface coastal band each year on May 15th, when the SST change attributed to the shading is strongest (Figure 1). The floats are advected backward in time for 30 days by the daily-average modeled currents using the ROMS offline tool (Capet et al., 2004; Carr et al., 2008). Depth, temperature, nitrate, and oxygen concentrations are stored along the floats trajectories and compared for the two experiments.

2.5. Additional Data Sets

Various data sets are used to evaluate the model simulations. Monthly climatologies over the period 2008–2015 are computed from a multisensor merged 4 × 4 km surface chlorophyll product (Gohin et al., 2002, https://marine.copernicus.eu/) and from the merged, multisensor, 0.05° × 0.05° (~4 km) OSTIA SST (Donlon et al., 2012). The CARS (0.5° × 0.5°) nutrient, temperature (Grados et al., 2018), and DO (Graco et al., 2020) high-resolution (0.1° × 0.1°) climatologies produced by the Instituto del Mar del Peru (IMARPE) are used for the evaluation of modeled cross-shore temperature and DO structures, respectively.

3. Model Evaluation

The control model simulation (NSH) is first evaluated against observations (see Figures in the Supporting Information S1). The model SST displays a typical upwelling pattern and compares well to OSTIA SST. A relatively weak (<0.5°C–1°C) negative SST bias is found off central Peru (Figure S2). The cross-shore temperature structure agrees well with the observed climatology (Figure S3). However, the upward slope of isotherms near the coast tends to be too steep near the coast. Consequently, a negative temperature bias (<0.5°C–1°C) is found near the surface (0–10 m). In contrast, the modeled temperature is too warm below 20 m, with the bias reaching a maximum of ~1°C offshore at ~60-m depth. The model thermocline is slightly too diffuse.

The modeled surface geostrophic EKE displays an alongshore band of high EKE between 8°S and 15°S extending westward south of 15°S, as in the observed EKE (Figure S4). However, modeled EKE levels are weaker as the intraseasonal forcing associated with remotely forced coastal-trapped waves (Echevin et al., 2014) and intraseasonal wind variability (Dewitte et al., 2011) are not included in the monthly climatological forcing.

Expectedly, the model surface chlorophyll is high along the coast and decreases offshore (Figure S5). The nearshore chlorophyll bias is positive (~5 mg Chl m^{-3} bias in ~50 km band) off Northern Peru (6°S–10°S). The offshore modeled nitracline depth (~40–60 m) is well positioned but isopleths tend to slope too steeply toward the coast (Figure S6). The near-surface nearshore (0–50-m depth, 0–200 km) nitrate bias reaches ~8–10 μmol kg^{-1}, a discrepancy found in several ROMS and CROCO-PISCES simulations in the region (e.g., Echevin et al., 2008; Espinoza et al., 2017; Hauschildt et al., 2021). The upper part (50–200 m) of the OMZ is well reproduced (Figure S7): DO bias is only ~10–30 μmol kg^{-1} in the upper part of the OMZ. Modeled DO concentrations tend to be slightly lower than the observed at depths greater than ~100 m, but the latter are known to be ~5–10 μmol kg^{-1} higher than real values in the OMZ core (Bianchi et al., 2012; Espinoza-Morriberon et al., 2019; Fuenzalida et al., 2009). Overall, the model physical and biogeochemical biases are limited and using this model configuration to investigate the impact of chlorophyll shading is a sound approach.

4. Impacts of the Chlorophyll Shading

Chlorophyll shading impacts both surface and subsurface water properties. The shading effect induces a warming of surface waters offshore (<0.5°C) and a cooling within ~100–300 km from the coast (Figure 1a). The strongest cooling (~1°C) occurs along the central shelf (9°S–13°S) and is strongest in austral fall (Figure 1b).

The subsurface structure of the coastal upwelling system is modified. A subsurface cooling (~1.2°C–1.5°C) produced by the shading effect is centered at ~20-m depth nearshore and ~50-m depth offshore (Figure 2d), enhancing the stratification in the upper thermocline (see red lines spacing in Figure 2a). The enhanced upper thermocline induces a shoaling of the mixed layer (Figure 1c), and reduces the nearshore isotherm slope (near 10–50-m depth; see red lines in Figure 2a) and the associated cross-shore pressure gradient (through the thermal wind relation, not shown).

Consequently, the surface equatorward current and the poleward Peru Chile Under Current (hereafter PCUC) decrease by ~3 cm s^{-1} (10%–20% with respect to NSH) near 10–20-m depth and by ~0.5 cm s^{-1} (15%–25%) near 100–200-m depth, respectively (Figure 2f). This reduces the current vertical shear driving baroclinic instability (e.g., Colas et al., 2012; Echevin et al., 2011) and induces a ~25% decrease of the surface geostrophic EKE over the central Peru shelf and slope (Figure S4). In contrast, although the depth-integrated Ekman transport is unchanged, the wind-driven cross-shore current is enhanced (Figures 2b and 2e) because of the thinner Ekman layer induced by the stronger stratification (not shown).

Shading-induced changes in stratification and circulation also modify surface and subsurface biogeochemical properties. Nearshore surface chlorophyll increases (~1–2 mg Chl m^{-3} i.e., ~50% increase) off the central shelf (5°S–14°S) and decreases north of 4°S (Figure 3a). The surface chlorophyll increase is maximum in austral spring (Figure 3b). The cross-shore chlorophyll structure reveals an increase in the surface layer (~0–10 m) offshore (20–200 km) and a decrease nearshore (~20-km band; Figures 4a and 4d). The stratification change induces a shoaling of the nitracline (marked by the 22–24 μmol kg^{-1} isopleths; Figure 4b) and a shoaling of the oxycline (Figure 4c): quasi-anoxic waters (i.e., DO < 10 μmol kg^{-1}) reach the shelf in SH (Figures 4c and 4f). This lower DO concentration on the shelf is consistent with the weaker PCUC (Figure 2f), which ventilates the OMZ less efficiently (e.g., Espinoza et al., 2019; Montes et al., 2010, 2014). Furthermore, the nearly anoxic waters on the shelf may modify the nitrogen cycle and induce denitrification, leading to a nearshore subsurface nitrate loss (Figure 4e).

The changes in the subsurface circulation have a weak impact on the pathways of the source waters (SW) upwelled over the shelf over a period of one month before upwelling, as water parcels follow broadly similar pathways in the two simulations (Figure S8). The SW depth range being relatively shallow (~5–35 m, Table 1), SW temperature is clearly impacted by the change in solar penetration. The SW average temperature difference is relatively large (~1°C) and remains approximately constant over the period (Table 1). The SW mean depth is ~2–2.5 m shallower in SH (Table 1), which can be expected because of the increased nearshore stratification (e.g., Oerder et al., 2015). The SW nitrate content is ~2 μmol kg^{-1} lower in SH, as SW are located above the nutricline, where nitrate concentration has decreased in SH (Figure 4e; 10–30-m depth range). The occurrence of the chlorophyll increase (Figure 3) in spite of a weak nitrate decrease in

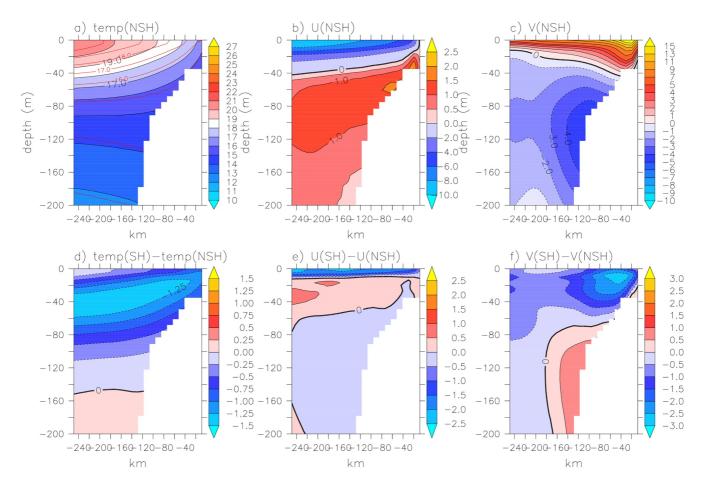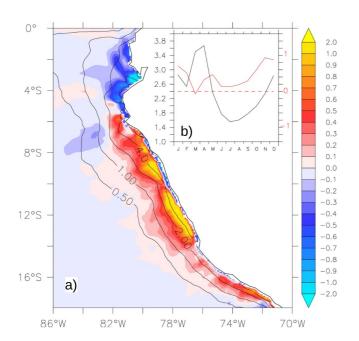**Figure 2.** Mean cross-shore structure of (a) temperature (NSH; in °C); (b) cross-shore current (NSH; in cm s⁻¹; positive shoreward); (c) alongshore current (NSH; in cm s⁻¹; positive equatorward). Variations (SH-NSH) in the mean cross-shore (d) temperature; (e) cross-shore current; (f) alongshore current. Red lines in (a) indicate the position of SH isotherms (13°C–20°C, with 1°C spacing) and highlight the upward shift of isotherms in SH. Variables are averaged alongshore between 8°S and 13°S.

SH remains to be explained. The seasonal evolution of the light limiting factor averaged over a coastal band (Figure S9) shows that the mixed layer shoaling (Figure 1) mitigates light limitation and increases surface primary productivity in April and December, and that other biogeochemical and physical mechanisms drive the surface chlorophyll temporal evolution over the rest of the year. Analyzing the SH and NSH phytoplankton budgets would be necessary to investigate the processes at stake in more details.

5. Discussion and Conclusions

The cooling effect of the shading in the Peruvian coastal upwelling can be explained as follows: when the shading effect is active, the layer located below the chlorophyll-rich layer, which contains a significant portion of the upwelling source waters, is not heated by solar radiation. Conversely, when the shading effect is not active, solar radiation reaches a larger depth range and warms a greater portion of the source waters. Consequently, source waters become colder in SH with respect to NSH as they transit toward the high-chlorophyll coastal region. The impact on SST is enhanced at the end of austral summer as surface chlorophyll reaches its highest levels in the Peru upwelling system (Echevin et al., 2008; Pennington et al., 2006, Figure 3b), leading to the highest SST difference around austral summer (∼−0.7°C; Figure 1b). The modeled NHCS SST cooling is stronger than that simulated in the Senegal and Benguela upwelling systems by Hernandez et al. (2017) (∼−0.3°C, see their Figure 6), possibly because of the low resolution (25 km) in their ocean model and the absence of feedback of the shading effect on the prescribed chlorophyll fields.

Figure 3. (a) Mean surface chlorophyll difference (SH-NSH; in mg Chl m^{-3}; color scale) and mean surface chlorophyll (NSH; in mg Chl m^{-3}; contours); (b) Seasonal cycle of surface chlorophyll (NSH; black line) and chlorophyll difference (SH-NSH; red line) in the coastal box (see black lines in Figure 1a).

SST is a straightforward and useful metric for the evaluation of EBUS regional models (e.g., Penven et al., 2005 in the NHCS). A nearshore cold bias has been reported in several EBUS regional simulations (e.g., Colas et al., 2012; Dufois et al., 2012; Veitch et al., 2009, 2010; Figure S2). It has been attributed to either an observational warm bias in SST satellite observations (e.g., Dufois et al., 2012) or to overly strong nearshore winds in satellite-derived model forcing, as nearshore wind (or wind stress) values are generally interpolated from the offshore reliable scatterometer measurements into the so-called ~25–50-km-wide nearshore "satellite blind zone" lacking accurate observations (e.g., Bentamy et al., 2021; Capet et al., 2004). The too strong alongshore winds may then drive a too intense coastal upwelling, transporting overly deep and cold source waters to the surface in the models.

Reducing SST model bias in EBUS has motivated the use of regional atmospheric models (e.g., Chamorro et al., 2018, 2021) and regional ocean-atmosphere coupled models (e.g., Oerder et al., 2016, 2018) to correctly represent the nearshore wind drop-off. As the chlorophyll shading effect induces a marked SST decrease near the coast, surface cooling could induce a stabilization of the marine boundary layer hence a reduction of the alongshore surface wind and latent heat flux (e.g., Jin et al., 2009; Perlin et al., 2007). This would subsequently reduce coastal upwelling but would increase offshore (50–100 km from the coast) upwelling driven by Ekman suction (e.g., Albert et al., 2010) associated with the enhanced wind drop-off. Consequently, offshore productivity could be stimulated more than nearshore productivity in the coupled simulations. However, such complex mechanisms need to be studied in more details using dedicated high-resolution ocean-atmosphere-biogeochemical coupled model experiments. Note also that the shading effect studied in the present work was performed using an ocean model forced by wind stress and SST restoring. Using heat fluxes and wind stress computed from bulk formulae may lead to a different (dampened) SST change and remains to be investigated.

The subsurface cooling associated with the shading effect also strongly impacts the biogeochemical system: as thermal stratification is enhanced and more realistic in the surface layer, vertical mixing is reduced and the vertical gradients of biogeochemical properties are modified. The shading effect impacts differently on the nearshore NHCS biogeochemical biases: the positive nitrate bias (Figure S5) in the surface layer is almost unchanged, whereas the upper OMZ bias is slightly reduced (Figure S6). The presence of nearly anoxic bottom waters (DO < 10 μmol kg^{-1}) over the shelf (Figures 4c and S6) has been reported (e.g., Kalvelage et al., 2013; Revsbech et al., 2009; Thomsen et al., 2016). In contrast, the nearshore surface chlorophyll bias increases (Figure S4) even though uncertainties in the satellite estimations of surface chlorophyll remain high (e.g., Echevin et al., 2008). Thus, the impact of the shading effect on the model biogeochemical bias shows that it needs to be taken into account when model parameter tuning is performed, in order to avoid possible compensation of errors.

Last, the shading effect also impacts on the nearshore mesoscale circulation, known to feedback on surface productivity, subsurface nutrient and oxygen distribution in EBUS (e.g., Gruber et al., 2011; Lathuilière et al., 2010). The mesoscale turbulence decrease induced by the shading effect would mitigate the offshore, downward transport of upwelled nutrients due to eddy quenching, and enhance nearshore productivity. Submesoscale processes may also modulate the shading effect. In the California upwelling system, they tend to reduce plankton biomass in the productive coastal region (i.e., ~100-km-wide coastal band) and increase it dramatically offshore (Kessouri et al., 2020). An increase of the offshore surface chlorophyll may increase the shading-induced cooling of subsurface and upwelled waters. On the other hand, the shading-induced reduction (~25%) of nearshore EKE may partly mitigate the subduction of nutrients induced by submesoscale eddies and hence partly compensate for the reduction of nearshore

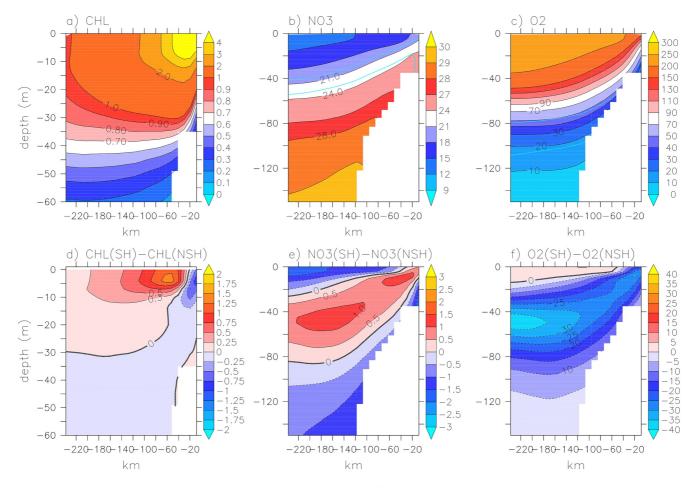**Figure 4.** Mean cross-shore structure of (a) chlorophyll structure (NSH; in mg Chl m⁻³); (b) nitrate (NSH; in µmol kg⁻¹; 22 and 24 µmol kg⁻¹ isopleths in SH are marked by white isolines); (c) dissolved oxygen (SH; in µmol kg⁻¹; 10 and 30 µmol kg⁻¹ isopleths in SH are marked by cian isolines); variations (SH-NSH) in the mean cross-shore (d) chlorophyll; (e) nitrate; (f) oxygen.

productivity reported in Kessouri et al. (2020). In any case, other modeling studies, resolving submesoscale processes and forced by intraseasonal boundary conditions and winds, are needed to confirm the effect of the shading effect on eddy-fluxes in a more realistic context. Such sensitivity experiments, which are beyond the scope of the present study, may help disentangling the complex nonlinear mechanisms at stake.

To conclude, the shading effect, a mechanism as of today disregarded in EBUS regional eddy-resolving modeling studies, strongly impacts the physical and biogeochemical functioning of the Peruvian ecosystem. As this process depends on the strength of nearshore chlorophyll surface concentration, impacts are also expected in the Canary and Benguela EBUS where surface chlorophyll is higher (e.g., Thomas et al., 2001) than in the California and Chile EBUS. This remains to be investigated in future work following the approach described in the present study.

Table 1
Depth, Temperature, Nitrate, and Dissolved Oxygen Concentration of Upwelling Source Water Parcels, 30 and 15 Days Before They are Upwelled in the Nearshore Surface Layer in Mid-May (Time of the Maximum SST Difference, See Figure 1b)

Exp#	Time before upw	Depth (m)	Temperature (°C)	Nitrate (µmol kg⁻¹)	Oxygen (µmol kg⁻¹)
NSH	30 days	21.5 ± 16.1	17.0 ± 1.5	25.2 ± 4.9	54.5 ± 65
SH	30 days	19.0 ± 17.0	16.1 ± 1.3	23.3 ± 5.2	57.0 ± 67
NSH	15 days	18.9 ± 12.0	17.2 ± 1.3	24.4 ± 4.5	68 ± 68
SH	15 days	16.8 ± 12.6	16.3 ± 1.3	22.8 ± 4.6	66 ± 69

Conflict of Interest

The authors declare no conflicts of interest relevant to this study.

Data Availability Statement

The code can be freely downloaded at https://doi.org/10.5281/zenodo.4792452. Model climatologies and scripts to reproduce the article's figures can be freely downloaded at https://doi.org/10.5281/zenodo.5175978.

References

Albert, A., Echevin, V., Lévy, M., & Aumont, O. (2010). Impact of nearshore wind stress curl on coastal circulation and primary productivity in the Peru upwelling system. *Journal of Geophysical Research*, *115*, C12033. https://doi.org/10.1029/2010JC006569

Anderson, W. G., Gnanadesikan, A., Hallberg, R., Dunne, J., & Samuels, B. L. (2007). Impact of ocean color on the maintenance of the Pacific Cold Tongue. *Geophysical Research Letters*, *34*, L11609. https://doi.org/10.1029/2007GL030100

Aumont, O., & Bopp, L. (2006). Globalizing results from ocean in situ iron fertilization studies. *Global Biogeochemical Cycles*, *20*, GB2017. https://doi.org/10.1029/2005GB002591

Aumont, O., Ethé, C., Tagliabue, A., Bopp, L., & Gehlen, M. (2015). PISCES-v2: an ocean biogeochemical model for carbon and ecosystem studies. *Geoscientific Model Development*, *8*, 2465–2513. https://doi.org/10.5194/gmd-8-2465-2015

Barnier, B., Siefridt, L., & Marchesiello, P. (1995). Thermal forcing for a global ocean circulation model using a three-year climatology of ECMWF analyses. *Journal of Marine Systems*, *6*, 363–380. https://doi.org/10.1016/0924-7963(94)00034-9

Becker, J. J., Sandwell, D. T., Smith, W. H. F., Braud, J., Binder, B., Depner, J., et al. (2009). Global bathymetry and elevation data at 30 arc seconds resolution: SRTM30_PLUS. *Marine Geodesy*, *32*(4), 355–371. https://doi.org/10.1080/01490410903297766

Bentamy, A., Grodsky, S. A., Cambon, G., Tandeo, P., Capet, X., Roy, C., et al. (2021). Twenty-Seven years of scatterometer surface wind analysis over eastern boundary upwelling systems. *Remote Sensing*, *13*, 940. https://doi.org/10.3390/rs13050940

Bianchi, D., Dunne, J. P., Sarmiento, J. L., & Galbraith, E. D. (2012). Data-based estimates of suboxia, denitrification, and N_2O production in the ocean and their sensitivities to dissolved O_2. *Global Biogeochemical Cycles*, *26*, GB2009. https://doi.org/10.1029/2011GB004209

Capet, X. J., Marchesiello, P., & McWilliams, J. C. (2004). Upwelling response to coastal wind profiles. *Geophysical Research Letters*, *31*, L13311. https://doi.org/10.1029/2004GL020123

Carr, S. D., Capet, X. J., McWilliams, J. C., Pennington, J. T., & Chavez, F. (2008). The influence of diel vertical migration on zooplankton transport and recruitment in an upwelling region: Estimates from a coupled behavioral-physical model. *Fisheries Oceanography*, *17*(1), 1–15. https://doi.org/10.1111/j.1365-2419.2007.00447.x

Chamorro, A., Echevin, V., Colas, F., Oerder, V., Tam, J., & Quispe-Ccalluari, C. (2018). Mechanisms of the intensification of the up-welling-favorable winds during El Niño 1997–1998 in the Peruvian upwelling system. *Climate Dynamics*, *51*, 3717–3733. https://doi.org/10.1007/s00382-018-4106-6

Chamorro, A., Echevin, V., Dutheil, C., TamGutierrez, J. D., Colas, F., & Colas, F. (2021). Projection of upwelling-favorable winds in the Peruvian upwelling system under the RCP8.5 scenario using a high-resolution regional model. *Climate Dynamics*, *57*, 1–16. https://doi.org/10.1007/s00382-021-05689-w

Colas, F., Capet, X., McWilliams, J., & Li, Z. (2012). Mesoscale eddy buoyancy flux and eddy-induced circulation in Eastern Boundary currents. *Journal of Physical Oceanography*, *43*(6), 1073–1095. https://doi.org/10.1175/JPO-D-11-0241.1

da Silva, A. M., Young-Molling, C. C., & Levitus, S. (1994). *Atlas of surface marine data 1994, vol. 1, algorithms and procedures*. NOAA Atlas NESDIS (Vol. 6, pp. 83). MD: NOAA, Silver Spring.

Dewitte, B., Illig, S., Renault, L., Goubanova, K., Takahashi, K., Gushchina, D., et al. (2011). Modes of covariability between sea surface temperature and wind stress intraseasonal anomalies along the coast of Peru from satellite observations (2000–2008). *Journal of Geophysical Research*, *116*, C04028. https://doi.org/10.1029/2010JC006495

Donlon, C. J., Martin, M., Stark, J., Roberts-Jones, J., Fiedler, E., & Wimmer, W. (2012). The operational sea surface temperature and sea ice analysis (OSTIA) system. *Remote Sensing of Environment*, *116*, 140–158. https://doi.org/10.1016/j.rse.2010.10.017

Dufois, F., Penven, P., Peter Whittle, C., & Veitch, J. (2012). On the warm nearshore bias in pathfinder monthly SST products over eastern boundary upwelling systems. *Ocean Modelling*, *47*, 113–118. https://doi.org/10.1016/j.ocemod.2012.01.007

Echevin, V., Albert, A., Lévy, M., Graco, M., Aumont, O., Piétri, A., & Garric, G. (2014). Intraseasonal variability of nearshore productivity in the Northern Humboldt current system: The role of coastal trapped waves. *Continental Shelf Research*, *73*, 14–30. https://doi.org/10.1016/j.csr.2013.11.015

Echevin, V., Aumont, O., Ledesma, J., & Flores, G. (2008). The seasonal cycle of surface chlorophyll in the Peruvian upwelling system: A modelling study. *Progress in Oceanography*, *79*(2–4), 167–176. https://doi.org/10.1016/j.pocean.2008.10.026

Echevin, V., Colas, F., Chaigneau, A., & Penven, P. (2011). Sensitivity of the Northern Humboldt current system nearshore modeled circulation to initial and boundary conditions. *Journal of Geophysical Research*, *116*, C07002. https://doi.org/10.1029/2010JC006684

Espinoza-Morriberon, D., Echevin, V., Colas, F., Tam, J., Gutierrez, D., Graco, M., et al. (2019). Oxygen variability during ENSO in the tropical south eastern pacific. *Frontiers in Marine Science*, *5*, 526. https://doi.org/10.3389/fmars.2018.00526

Espinoza-Morriberón, D., Echevin, V., Colas, F., Tam, J., Ledesma, J., Vásquez, L., & Graco, M. (2017). Impacts of El Niño events on the Peruvian upwelling system productivity. *Journal of Geophysical Research: Oceans*, *122*, 5423–5444. https://doi.org/10.1002/2016JC012439

FAO. (2017). *Global capture production database updated to 2015—Summary information*. FAO. Retrieved from http://www.fao.org/3/a-br186e.pdf

Ferry, N., Parent, L., Garric, G., Bricaud, C., Testut, C. E., Le Galloudec, O., & Molines, J. M. (2012). GLORYS2V1 global ocean reanalysis of the altimetric era (1992–2009) at meso scale. *Mercator Ocean–Quarterly Newsletter*, *44*.

Fuenzalida, R., Schneider, W., Graces-Vargas, J., Bravo, L., & Lange, C. (2009). Vertical and horizontal extension of the oxygen minimum zone in the eastern South Pacific Ocean. *Deep Sea Research Part II: Topical Studies in Oceanography*, *56*(16), 992–1003. https://doi.org/10.1016/j.dsr2.2008.11.001

Gohin, F., Druon, J. N., & Lampert, L. (2002). A five channel chlorophyll concentration algorithm applied to SeaWiFS data processed by SeaDAS in coastal waters. *International Journal of Remote Sensing*, *23*(8), 1639–1661. https://doi.org/10.1080/01431160110071879

Graco, M., Anculle, T., Chaigneau, A., Ledesma, J., Flores, G., Morón, O., et al. (2020). *Variabilidad espacial y temporal del oxígeno disuelto y de la ZMO en el sistema de afloramien-to frente a Perú*. Boletín Instituto del Mar del Perú, Libro de la Anchoveta.

Grados, C., Chaigneau, A., Echevin, V., & Domínguez, N. (2018). Upper ocean hydrology of the Northern Humboldt current system at seasonal, interannual and interdecadal scales. *Progress in Oceanography*, *165*, 123–144. https://doi.org/10.1016/j.pocean.2018.05.005

Gruber, N., Frenzel, H., Doney, S. C., Marchesiello, P., McWilliams, J. C., Moisan, J. R., et al. (2006). Eddy-resolving simulation of plankton ecosystem dynamics in the California current system. *Deep Sea Research Part I: Oceanographic Research Papers*, *53*(9), 1483–1516. https://doi.org/10.1016/j.dsr.2006.06.005

Gruber, N., Lachkar, Z., Frenzel, H., Marchesiello, P., Münnich, M., McWilliams, J. C., et al. (2011). Eddy-induced reduction of biological production in eastern boundary upwelling systems. *Nature Geosciences*, *4*, 787–792. https://doi.org/10.1038/ngeo1273

Hauschildt, J., Thomsen, S., Echevin, V., Oschlies, A., José, Y. S., Krahmann, G., et al. (2021). The fate of upwelled nitrate off Peru shaped by submesoscale filaments and fronts. *Biogeosciences*, *18*, 3605–3629. https://doi.org/10.5194/bg-2020-112

Hernandez, O., Jouanno, J., Echevin, V., & Aumont, O. (2017). Modification of sea surface temperature by chlorophyll concentration in the Atlantic upwelling systems. *Journal of Geophysical Research: Oceans*, *122*, 5367–5389. https://doi.org/10.1002/2016JC012330

Hilt, M., Auclair, F., Benshila, R., Bordois, L., Capet, X., Debreu, L., et al. (2020). Numerical modelling of hydraulic control, solitary waves and primary instabilities in the Strait of Gibraltar. *Ocean Modelling*, *151*, 101642. https://doi.org/10.1016/j.ocemod.2020.101642

Jerlov, N. (1976). Index. In *Marine optics* (pp. 227–231). Elsevier Oceanography Series. https://doi.org/10.1016/s0422-9894(08)70809-2

Jin, X., Dong, C., Kurian, J., McWilliams, J. C., Chelton, D. B., & Li, Z. (2009). SST-wind interaction in coastal upwelling: Oceanic simulation with empirical coupling. *Journal of Physical Oceanography*, *39*, 2957–2970. https://doi.org/10.1175/2009JPO4205.1

Kalvelage, T., Lavik, G., Lam, P., Contreras, S., Arteaga, L., Loscher, C. R., et al. (2013). Nitrogen cycling driven by organic matter export in the south pacific oxygen minimum zone. *Nature Geosciences*, *6*(3), 228–234. https://doi.org/10.1038/ngeo1739

Kessouri, F., Bianchi, D., Renault, L., McWilliams, J. C., Frenzel, H., & Deutsch, C. A. (2020). Submesoscale currents modulate the seasonal cycle of nutrients and productivity in the California current system. *Global Biogeochemical Cycles*, *34*, e2020GB006578. https://doi.org/10.1029/2020GB006578

Key, R. M., Kozyr, A., Sabine, C. L., Lee, K., Wanninkhof, R., Bullister, J., et al. (2004). A global ocean carbon climatology: Results from GLODAP. *Global Biogeochemical Cycles*, *18*, GB4031. https://doi.org/10.1029/2004GB002247

Large, W. G., McWilliams, J. C., & Doney, S. (1994). Oceanic vertical mixing: A review and a model with a nonlocal boundary layer parameterization. *Reviews of Geophysics*, *32*, 363–403. https://doi.org/10.1029/94RG01872

Lathuilière, C., Echevin, V., Lévy, M., & Madec, G. (2010). On the role of the mesoscale circulation on an idealized coastal upwelling ecosystem. *Journal of Geophysical Research*, *115*, C09018. https://doi.org/10.1029/2009JC005827

Lemarié, F., Kurian, J., Shchepetkin, A. F., Molemaker, J., Colas, F., & McWilliams, J. C. (2012). Are there inescapable issues prohibiting the use of terrain-following coordinates in climate models? *Ocean Modelling*, *42*, 57–79. https://doi.org/10.1016/j.ocemod.2011.11.007

Lengaigne, M., Menkes, C., Aumont, O., Gorgues, T., Bopp, L., André, J. M., & Madec, G. (2007). Influence of the oceanic biology on the tropical Pacific climate in a coupled general circulation model. *Climate Dynamics*, *28*(5), 503–516. https://doi.org/10.1007/s00382-006-0200-2

Lin, P., Liu, H., & Zhang, X. (2007). Sensitivity of the upper ocean temperature and circulation in the equatorial Pacific to solar radiation penetration due to phytoplankton. *Advanced Atmospheric Sciences*, *24*, 765–780. https://doi.org/10.1007/s00376-007-0765-7

Loeptien, U., Eden, C., Timmermann, A., & Dietze, H. (2009). Effects of biologically induced differential heating in an eddy-permitting coupled ocean-ecosystem model. *Journal of Geophysical Research: Oceans*, *114*, C06011. https://doi.org/10.1029/2008JC004936

Manizza, M., Le Quéré, C., Watson, A. J., & Buitenhuis, E. T. (2005). Bio-optical feedbacks among phytoplankton, upper ocean physics and sea-ice in a global model. *Geophysical Research Letters*, *32*, L05603. https://doi.org/10.1029/2004GL020778

Marchesiello, P., Debreu, L., & Couvelard, X. (2009). Spurious diapycnal mixing in terrain-following coordinate models: The problem and a solution. *Ocean Modelling*, *26*(3–4), 156–169. https://doi.org/10.1016/j.ocemod.2008.09.004

Marchesiello, P., McWilliams, J. C., & Shchepetkin, A. (2003). Equilibrium structure and dynamics of the California current system. *Journal of Physical Oceanography*, *33*(4), 753–783. https://doi.org/10.1175/1520-0485(2003)33%3C753:ESADOT%3E2.0.CO;2

Messié, M., & Chavez, F. P. (2015). Seasonal regulation of primary production in eastern boundary upwelling systems. *Progress in Oceanography*, *134*, 1–18. https://doi.org/10.1016/j.pocean.2014.10.011

Montes, I., Colas, F., Capet, X., & Schneider, W. (2010). On the pathways of the equatorial subsurface currents in the eastern equatorial Pacific and their contributions to the Peru-Chile Undercurrent. *Journal of Geophysical Research*, *115*, C09003. https://doi.org/10.1029/2009JC005710

Montes, I., Dewitte, B., Gutknecht, E., Paulmier, A., Dadou, I., Oschlies, A., & Garçon, V. (2014). High-resolution modeling of the eastern tropical pacific oxygen minimum zone: Sensitivity to the tropical oceanic circulation. *Journal of Geophysical Research: Oceans*, *119*, 5515–5532. https://doi.org/10.1002/2014JC009858

Oerder, V., Colas, F., Echevin, V., Codron, F., Tam, J., & Belmadani, A. (2015). Peru-Chile upwelling dynamics under climate change. *Journal of Geophysical Research: Oceans*, *120*, 1152–1172. https://doi.org/10.1002/2014JC010299

Oerder, V., Colas, F., Echevin, V., Masson, S., Hourdin, C., Jullien, S., et al. (2016). Mesoscale SST-wind stress coupling in the Peru-Chile current system: Which mechanisms drive its seasonal variability? *Climate Dynamics*, *47*, 2309–2330. https://doi.org/10.1007/s00382-015-2965-7

Oerder, V., Colas, F., Echevin, V., Masson, S., & Lemarié, F. (2018). Impacts of the mesoscale ocean-atmosphere coupling on the Peru-Chile ocean dynamics: The current-induced wind stress modulation. *Journal of Geophysical Research: Oceans*, *123*, 812–833. https://doi.org/10.1002/2017JC013294

Park, J. Y., Kug, J. S., Seo, H., & Bader, J. (2014). Impact of bio-physical feedbacks on the tropical climate in coupled and uncoupled GCMs. *Climate Dynamics*, *43*(7–8), 1811–1827. https://doi.org/10.1007/s00382-013-2009-0

Paulmier, A., & Ruiz-Pino, D. (2009). Oxygen minimum zones (OMZs) in the modern ocean. *Progress in Oceanography*, *80*(3–4), 113–128. https://doi.org/10.1016/j.pocean.2008.08.001

Paulson, C. A., & Simpson, J. J. (1977). Irradiance measurements in the upper ocean. *Journal of Physical Oceanography*, *7*, 952–956. https://doi.org/10.1175/1520-0485(1977)007<0952:imituo>2.0.co;2

Pennington, J. T., Mahoney, K. L., Kuwahara, V. S., Kober, D. D., Calienes, R., & Chavez, F. P. (2006). Primary production in the eastern tropical pacific: A review. *Progress in Oceanography*, *69*(2–4), 285–317. https://doi.org/10.1016/j.pocean.2006.03.012

Penven, P., Debreu, L., Marchesiello, P., & McWilliams, J. C. (2006). Evaluation and application of the ROMS 1-way embedding procedure to the central California upwelling system. *Ocean Modelling*, *12*(1–2), 157–187. https://doi.org/10.1016/j.ocemod.2005.05.002

Penven, P., Echevin, V., Pasapera, J., Colas, F., & Tam, J. (2005). Average circulation, seasonal cycle, and mesoscale dynamics of the Peru current system: A modeling approach. *Journal of Geophysical Research*, *110*, C10021. https://doi.org/10.1029/2005JC002945

Perlin, N., Skyllingstad, E. D., Samelson, R. M., & Barbour, P. L. (2007). Numerical simulation of air-sea coupling during coastal upwelling. *Journal of Physical Oceanography*, *37*(8), 2081–2093. https://doi.org/10.1175/JPO3104.1

Revsbech, N. P., Larsen, L. H., Gundersen, J., Dalsgaard, T., Ulloa, O., & Thamdrup, B. (2009). Determination of ultra-low oxygen concentrations in oxygen minimum zones by the STOX sensor. *Limnology and Oceanography: Methods*, *7*(5), 371–381. https://doi.org/10.4319/lom.2009.7.371

Ridgway, K. R., Dunn, J. R., & Wilkin, J. L. (2002). Ocean interpolation by four-dimensional least squares-Application to the waters around Australia. *Journal of Atmospheric and Oceanic Technology*, *19*(9), 1357–1375. https://doi.org/10.1175/1520-0426(2002)019<1357:oibfdw>2.0.co;2

Shchepetkin, A. F., & McWilliams, J. C. (2003). A method for computing horizontal pressure-gradient force in an oceanic model with a nonaligned vertical coordinate. *Journal of Geophysical Research*, *108*(C3), 3090. https://doi.org/10.1029/2001JC001047

Shchepetkin, A. F., & McWilliams, J. C. (2005). The regional oceanic modeling system (ROMS): A split-explicit, free-surface, topography-following-coordinate oceanic model. *Ocean Modelling*, *9*, 347–404. https://doi.org/10.1016/j.ocemod.2004.08.002

Tegen, I., & Fung, I. (1995). Contribution to the atmospheric mineral aerosol load from land surface modification. *Journal of Geophysical Research*, *100*, 18707–18726. https://doi.org/10.1029/95JD02051

Thomas, A. C., Carr, M.-E., & Strub, P. T. (2001). Chlorophyll variability in eastern boundary currents. *Geophysical Research Letters*, *28*, 3421–3424. https://doi.org/10.1029/2001GL013368

Thomsen, S., Kanzow, T., Colas, F., Echevin, V., Krahmann, G., & Engel, A. (2016). Do submesoscale frontal processes ventilate the oxygen minimum zone off Peru? *Geophysical Research Letters*, *43*, 8133–8142. https://doi.org/10.1002/2016GL070548

Veitch, J., Penven, P., & Shillington, F. (2009). The Benguela: A laboratory for comparative modeling studies. *Progress in Oceanography*, *83*(1–4), 296–302. https://doi.org/10.1016/j.pocean.2009.07.008

Veitch, J., Penven, P., & Shillington, F. (2010). Modeling equilibrium dynamics of the Benguela Current System. *Journal of Physical Oceanography*, *40*(9), 1942–1964. https://doi.org/10.1175/2010JPO4382.1